Characterization of Weld Bead Deposited on Low Carbon Steel Plate with TIG Welding Process

[1]Dr.T.Vigraman, [2]Chikatla Purna Chand, [3]K.G.N.S. Krishna Vara Prasad, [4]Pasupuleti Srinivas
[1]Professor, [2,3,4]Final year students, Department of Mechanical Engineering, Sasi Institute of Technology & Engineering, Tadepalligudem, Andhra Pradesh, India, [1]tvr@sasi.ac.in, [2]purnaachand011@gmail.com, [3]krishnakonda249@gmail.com, [4]srinivasupuleti333@gmail.com

Abstract - The characterization of weld bead deposited on low carbon steel plate with TIG welding is carried out in the present study. Three beads on plate deposits were made on a low carbon steel plate by setting the current at 75, 100 and 125 Amp, voltage at 40 Volt and the weld speed at 0.5 mm/s. The wire is fed at the rate of 2.67 mm/s. A 1.8 mm filler wire made with low carbon steel was used. The macroscopic and microscopic examination of the sample was carried out. The depth of penetration was more with respect to rise in current value for the selected weld speed. At the heat affected zone (HAZ) fine grains were seen, closer to the HAZ recrystalised grains were noted. At the base metal large ferrite grains with fine carbide particles dispersed along the grain boundaries are observed.

Keywords: Tungsten Inert Gas (TIG) welding, microscopic examination, macroscopic examination, Heat Affected Zone (HAZ), carbides and grains.

I. INTRODUCTION

The low carbon steel is used as a general purpose and structural material for boiler applications. The good mechanical properties such as moderate hardness, ductility, yield and tensile strength are in favour of selecting this material for various applications. Eswara Rao et al [1] discussed the effect of welding variables on the microstructure, mechanical properties of 5 mm thick plates of dissimilar grades of AISI 301 steel and 1020 steel. Ahmed Khalid Hussain et al [2] conducted experiments on the effect of welding speed on the tensile strength of Aluminum AA6351 alloy plate edges having single 'V' configuration, with different bevel angle and bevel heights. Karunakaran et al [3] compared the effect of pulsed current and constant current TIG welds on different physical properties and micro structural features of stainless steel. Selva Ganesh et al [4] performed TIG welding on dissimilar grades of steels SAE 2205 and AISI 304 steel and presented a maximum yield strength of 354 MPa and an ultimate tensile strength value of 549 MPa for the samples processed at 130 Amp. Arc welding is suitable for making high strength and high accuracy joints employed in pressure vessels and industrial applications. Manual metal arc welding is chosen for welding of dissimilar grades of steel and stainless steel to get a high quality and sound joints. Ankush Choudary et al (5) performed submerged welding to manufacture offshore structures owing to its high deposition rate and high weld quality.

TIG welding is more suitable for varying heat input and suitable for making pure joints. TIG welding is more expensive because it uses inert gas as shielding gas to protect the arc. . Kamlesh kumar et al [6] performed TIG welding on Ti-6Al-4V alloy inside a Argon gas chamber to obtain high quality joints free from oxides. Argon, carbon di oxide and helium is used as shielding gas to provide protective environment around the arc. Further, the plasma formed between the electrode and the base metal acts as a media to transfer energy from the electrode to the base metal. Widely pure argon gas is used as inert gas, sometimes it is mixed with helium and used as inert gas. Honma et al [7] investigated the optimum conditions of semi-automatic TIG welding parameters like wire diameter, feeding conditions, torch angle, wire feed angle and their effect on bead formation. Sathish et al [8] studied the feasibility of TIG welding process for joining ferrous and nonferrous materials. Further, welding of similar and dissimilar metals using TIG welding process was studied. Generally, TIG welding is carried out in pressure vessels to make root pass weld to ensure high quality, oxide free joints. In aircrafts TIG welding is applied to ensure oxide free, high quality joints therefore, wherever welded joints are required in aircrafts, they are made with TIG welding process.

II. EXPERIMENTAL PROCEDURE

A carriage consisting of a frame for rigidity and a base plate to support the other elements in the system with four wheels is designed and fabricated. Each wheel is powered by a direct current (DC) motor and arranged in such a manner that it moves in a straight line. The base plate supports the battery, torch holder and a wire feeder. A single wire is fed through wire feeding mechanism which is kept at an angle of $60\text{-}70^0$. Wire passes through a pair of rotating cylindrical rollers, because of friction between

 DOI : 10.35291/2454-9150.2020.0368

the rollers and the wire, linear motion of the wire is achieved. One of the rollers is connected to a variable speed DC motor to provide power to the roller. A cantilever beam is constructed with steel flats and the Gas Tungsten Arc Welding torch is attached with the steel flats with steel bolts. In Fig.1, the developed TIG welder and the torch connected to the power source and the Argon gas cylinder is shown. The wire is fed at the centre of the arc, so that complete melting of the filler wire and base metals is ensured. The design ensures compact and light weight easy to maintain and suitable for making weld over a short distance. With this facility weld speed and wire feed rate can be varied.

Fig. 1 A photograph showing the TIG welding carriage with torch holder and wire feeder.

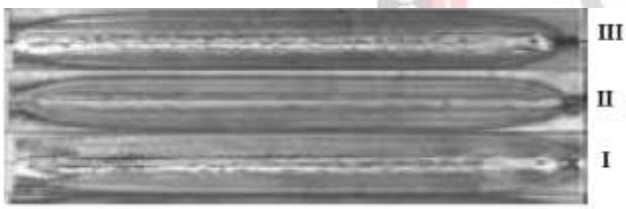

Fig. 2 Shows the beads formed on steel plate with TIG welding process.

The low carbon steel plate form is cut to the required size of 75 mm × 100 mm × 6 mm. The composition of the base metal and filler wire are presented in Table 1. A matching filler metal is used in the present work. TIG welding of the butt joints was carried out by varying the current value. The current values were set at 60, 75 and 100 Amp. The other two parameters welding voltage and welding speed were maintained at 40 V and 0.5 mm/s. The deposited bead on plate specimen was sectioned in the transverse direction to a cuboid of 75 mm × 10 mm × 6 mm. Conventional metallographic technique is adopted while polishing the specimens, for macroscopic and microscopic examinations. Nital is used as etchant to reveal grain boundaries. Further, both Nital and Picric acid is used to perform double etching to identify the presence of carbides. In Fig. 3 the sectioned and polished images of each deposited bead is shown.

Table 1 Elemental composition of low carbon steel and filler wire.

Item	Element	C	Fe	Mn	P	S
Base plate	Composition in wt. %	0.2	99.08	0.64	0.04	0.03
Wire	Composition in wt. %	0.15	99.11	0.64	0.05	0.05

Fig. 3 Macroscopic image of the three beads formed at various parameters.

III. RESULTS AND DISCUSSIONS

3.1 OPTICAL MACROSCOPY

The macrographs are shown in Fig.3; they are identified as I for 75, II for 100 and III for 125 Amp. For I, the weld metal was deposited at a current value of 100 Amp, voltage at 40 V and the weld speed at 0.5 mm/s. the wire feed rate was maintained at 2.67 mm/s for all the three deposits. The weld bead formed is not symmetric with respect to vertical axis for the macrograph I shown in Fig.3. The weld bead formed is almost symmetric for the macrograph II, with respect to the vertical axis as shown in Fig. 3. For the macrograph III, the weld bead is symmetric and the depth of penetration is maximum. The depth of penetration for I is least one for the weld bead made with current a current value of 75 Amp. As the weld current increases, the depth of penetration also increases which is evidenced in the macrographs I and II.

3.2 Optical Microscopy

The optical micrograph shown in Fig. 4 corresponds to the bead on plate shown in Fig. 3 marked as II. This specimen is etched with natal and picric acid to reveal the carbides. On top side of the micrograph, the weld metal is identified as grey regions having dark phase identified as carbides or pearlite. Complete fusion of the weld metal and base metal is evidenced with the micrographs shown in Fig. 4. The HAZ is distinctly visible with fine recrystallized grains. At the bottom side of the micrograph, at the base metal side white ferrite region is visible. The micrograph shown in Fig. 4 (b) presents the base metal microstructure. The average ferrite grain size is 20 µm. At the grain boundaries, grain boundary triple points and at few places at the grain matrix spherical particles are seen. These particles are identified as graphite particles. In Fig. 4(c) closer to the HAZ, these dendrites are finer and elongated. At the HAZ fine grains are seen, the average grain size is less than 10 µm. A thin line runs across the length of the micrograph which is parallel to the weld center line and this line is formed because of dynamic recrystallisation during cooling process. The

 DOI : 10.35291/2454-9150.2020.0368

recrystallised grain boundaries are connected together and runs as a line parallel the weld line.

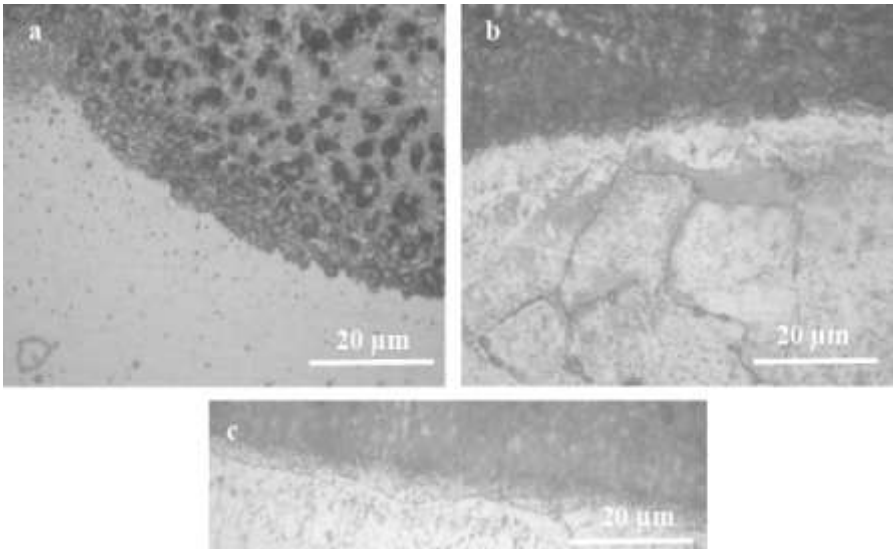

Fig. 4 a) The microstructure at the interface between the base metal and the bead, b) the microstructure at the circle 1 and c) the microstructure at the circle 2.

The optical micrograph shown in Fig. 5 corresponds to the bead on plate shown in Fig. 3 marked as III. At the bottom side of the micrograph, at the base metal side large ferrite grains are seen. At the grain boundaries, grain boundary triple points and at few places at the grain matrix spherical particles are seen. The base metal and the weld metal have exhibited complete coalescence and they are inseparable. Complete fusion of the weld metal and base metal is evidenced with the micrographs shown in Fig. 5. These particles are identified as graphite particles. In the micrograph as shown in Figure 5 (a), at the base metal side the average grain size is approximately 20 µm. In the Figure 5 (a), at the weld metal side columnar grains are seen, these grains are formed during solidification of the molten metal. Also, fine needle like structure is observed along with columnar α- grains. The micrograph shown in Fig. 5 (b) is for the region marked as 1 inside the red circle in the micrograph (a). In Fig. 5 (b) the dendritic structure is shown. Primary and secondary dendritic growth is revealed in this micrograph. The micrograph shown in Fig. 5 (c) is for the region marked as 2 inside the red circle in the micrograph (a). In Fig. 5 (c) closer to the HAZ, these dendrites are finer and elongated. At the HAZ fine grains are seen, the average grain size is less than 10 µm.

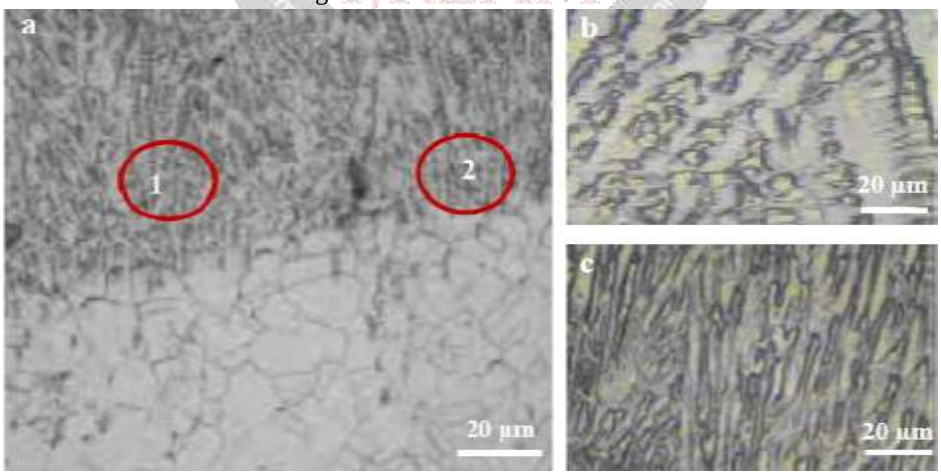

Fig. 5 a) The microstructure at the interface between the base metal and the bead, b) the microstructure at the circle 1 and c) the microstructure at the circle 2.

IV. CONCLUSIONS

A TIG welding carriage with wire feeder is designed and fabricated. This facility is useful to perform bead on plate experiments on low carbon steel plates. Three beads on plate deposits were made on a low carbon steel plate by setting the current at 75, 100 and 125 Amp, voltage at 40 Volt and the weld speed at 0.5 mm/s. The wire is fed at the rate of 2.67 mm/s. Complete fusion of the weld metal and base metal is evidenced with the micrographs. At the grain boundaries, grain boundary triple points and at few places at the grain matrix spherical particles are seen. At higher weld current, the weld bead is symmetric and the

 DOI : 10.35291/2454-9150.2020.0368

depth of penetration is maximum in comparison with the weld bead formed at lower current value.

REFERENCES

[1] Satish.T, Seenu.s, Shankarsiva.S, Design and Fabrication of Tig
Welding Machine, 2019, 7(6), 1-5.

[2] Hussain Ahmed Khalid, Lateef Abdul, Javed Mohd., Pramesh.T, "Influence of welding speed on tensile strength of welding joint in TIG welding process", International Journal of Applied Engineering Research, 2010, 1(3),1-8.

[3] Talabi,S.I, Adebesi,J.A.,Yahaya.T.,"Effect of welding variables on mechanical properties of low carbon steel welded joints ", Advances in Production Engineering & Management 2014, 9(4),181-185.

[4] Selva Ganesh C, Dr.Vigraman T, Sujith D, Velmanikandan M and Vetrivel T, "Microstructural and Transient Thermal Analysis of TIG Welded Joint SAE 2205 with AISI 304 with AISI 308 Filler Metal" International Journal of Engineering Technologies and Management Research, 2017, 4(10), 15-25.

[5] Karunakaran N., Effect of Pulsed Current on Temperature Distribution, Weld Bead Profiles and Characteristics of GTA Welded Stainless Steel Joints, International Journal of Engineering and Technology, 2012, 4(6),1-8.

[6] Narang H.K., Mahapatra M.M., Jha P.K., Prediction of the weld pool geometry of TIG arc welding using fuzzy logic controller, International Journal of Engineering, Science and Technology, 2011, 3(9),77-85.

[7] Abhimanyu Chauhan, Dr.Y.B.Mathur ," Experimental Study on Autogenous TiG welding of Mild Steel Material Using Lathe Machine", International Journal on Reasearch Technologies in Mechanical and Electrical Engineering, 2018, 5(1)8-16.

[8] Honma S and Yasuda K, "Study of Semi-automatic TIG welding", Welding International, 2004,18:6, 450-455.

 DOI : 10.35291/2454-9150.2020.0368